Dalton Transactions

Transferrin-inspired iron delivery across the cell membrane using [(L2Fe)2(μ-O)] (L = chlorquinaldol) to harness anticancer activity of ferroptosis

Journal:	*Dalton Transactions*
Manuscript ID	DT-ART-08-2023-002517.R1
Article Type:	Paper
Date Submitted by the Author:	07-Nov-2023
Complete List of Authors:	Abeydeera, Nalin; Kent State University, Mudarmah, Khalil; Kent State University, Chemistry Pant, Bishnu; Kent State University Krause, Jeanette; University of Cincinnati, Chemistry Zheng, Yaorong; Kent State University, Huang, Songping; Kent State University, Department of Chemistry

Transferrin-inspired iron delivery across the cell membrane using [$(L_2Fe)_2(\mu$-O)] (L = chlorquinaldol) to harness anticancer activity of ferroptosis

Nalin Abeydeera,[a] Khalil Mudarmah,[a,c] Bishnu D. Pant,[a] Jeanette A. Krause,[b]* Yao-Rong Zheng,[a]* and Songping D. Huang[a]*

[a] Department of Chemistry and Biochemistry, Kent State University, Kent, OH 44240.
[b] Department of Chemistry, University of Cincinnati, Cincinnati, OH 45221-0172, USA.
[c] On leave from Department of Chemistry, Jazan University, Jazan, 45142, Saudi Arabia.

KEYWORDS: Ferroptosis; Cancer chemotherapy; Fenton catalyst; ROS signaling pathways

ABSTRACT: Although iron is a bio-essential metal, dysregulated iron acquisition and metabolism result in production of reactive oxygen species (ROS) due to the Fenton catalytic reaction, which activates ferroptotic cell death pathways. The lipophilic Fe(III)-chelator chlorquinaldol (L; i.e., 5,7-dichloro-8-hydroxy-2-methylquinoline) strongly favors the formation of a highly stable binuclear Fe(III) complex [$(L_2Fe)_2(\mu$-O)] (**1**) that can mimic the function of the Fe(III)-transferrin complex in terms of the strong binding to Fe(III) and facile release of Fe(II) when the metal center is reduced. It should be noted that the cellular uptake of **1** is not transferrin receptor-mediated but enhanced by the high lipophilicity of chlorquinaldol. Once **1** is transported across the cell membrane, Fe(III) can be reduced by ferric reductase or other cellular antioxidants to be released as Fe(II), which triggers the Fenton catalytic reaction, thus harnessing the anticancer activity of iron. As the result, this transferrin-inspired iron-delivery strategy significantly reduces the cytotoxicity of **1** in normal human embryonic kidney cells (HEK 293) and the hemolytic activity of **1** in human red blood cells (hRBCs), giving rise to the unique tumor-specific anticancer activity of this Fe(III) complex.

1. Introduction

Known as the Janus-faced micronutrient in biology, iron is essential to all forms of life on the one hand, and cytotoxic on the other hand.[1-3] Such dichotomy of iron stems from its single most prominent characteristic - redox activity that can play a vital role in cellular replication, metabolism, and growth, while possessing the ability to catalyze the Fenton reaction to produce reactive oxygen species (ROS).[4] The latter are known to be deleterious to cells by causing lipid peroxidation of membranes, oxidation of proteins, cleavage of DNA and even activation of apoptotic cell death pathways.[5,6] Consequently, evolution has granted biological cells sophisticated cellular machinery to handle with care the acquisition, transport across the cell membrane, and release of iron into the cytoplasm.[7,8] In this regard, the most remarkable example is presented by nature on utilizing the hard-soft acid-base (HSAB) principle to impart high extracellular stability of the Fe(III)-transferrin complex and ready intracellular release of Fe(II) when the metal center is reduced.[9,10] Specifically, in the transferrin receptor-mediated endocytosis of cellular iron uptake in mammalian cells, the extracellular Fe(III) is bound to apo-transferrin, an iron-transporter protein containing two homologous octahedral Fe(III)-binding pockets each formed by hard Lewis-base donor atoms, i.e., a N and 5 O atoms to render high affinity for Fe(III), which not only conceals the ionic character of Fe(III), but also shields it from interacting with O_2 to produce ROS, or with amino acids and/or other biomolecules to undergo demetallation by ligand exchange.[11] Once the Fe(III)-transferrin complex is transported across the cell membrane *via* the transferrin receptor-mediated endocytosis, Fe(II) - a softer Lewis acid, is released by the consecutive action of the proton pump to lower the pH in order to re-protonate the donor atoms, and the concomitant reduction of Fe(III) by ferric reductase and/or cellular antioxidants.[12,13]

This publication reports on the synthesis, structural characterization, and *in vitro* anticancer activity studies of a transferrin-inspired binuclear Fe(III) complex $[(L_2Fe)_2(\mu\text{-}O)]$ (**1**; where L = chlorquinaldol or 5,7-dichloro-8-hydroxy-2-methylquinoline) that can target the vulnerability of cellular iron uptake. We show that as a functional mimic of the Fe(III)-transferrin complex **1** can circumvent the tight regulation of iron uptake in cancer cells to penetrate the cell membrane, accumulate in mitochondria, and even enter the cell nucleus due to the high lipophilic nature of the ligand (log P = 3.55), thus disrupting the cellular iron homeostasis. As the result, **1** exhibits *in vitro* anticancer activity against cells from six different human cancer cell lines, attesting to its broad-spectrum and potent activity. Additionally, the cytotoxicity of **1** in normal human cells (i.e., HEK 293 cells) is lower as opposed to that in cancer cells and causes negligible hemolysis in human red blood cells (hRBCs), indicating that a wider therapeutic window may exist for **1** compared with cisplatin. Furthermore, **1** can overcome the Pt resistance in the phenotype of ovarian cancer cells that are known to have developed resistance to Pt (i.e., A2780cis cells). It should be noted that use of Fe complexes as anticancer agents has long been a field of intensive investigations after the *in vitro* anticancer activity of ferrocenium picrate and ferrocenium trichloroacetate was discovered in 1984 by Kopf-Maier and co-workers. [14] Thus far, a large number of anticancer Fe complexes have been reported in over 200 research articles, [15,16] but none of these have advanced to the stage of human clinical studies, which is in sharp contrast to compounds containing gallium - the so-called fake iron. [17-19] Recently, the antitumor mechanism of Fe(III) complexes as well as ferroptosis induced by other metal complexes as a new anticancer strategy have attracted increasing research attention as exemplified by several important reports. [20-22]

2. Material and Methods

Materials: Chemicals and reagents were commercial products and used as received. Specifically, chloroform, 5,7-dichloro-8-hydroxy-2-methylquinoline, dimethyl sulfoxide, ethanol, hydrochloric acid, iron nitrate nonahydrate, nitric acid, potassium carbonate and thiourea were all purchased from MilliporeSigma.

Synthesis of [$(L_2Fe)_2(\mu\text{-}O)$]: A solution of 5,7-dichloro-8-hydroxy-2-methylquinoline (0.3 mmol) in 20-mL ethanol containing K_2CO_3 (0.3 mmol) was added to a solution of $Fe(NO_3)_3 \cdot 9H_2O$ (0.1 mmol) in 10-mL ethanol, followed by vigorous stirring for 3 hours at 70°C. A yellowish-brown precipitate was formed. After filtration, the crystalline powder was washed with ethanol three times. After drying in a vacuum oven for 12 hours, 0.0517 g of the product was obtained (78% yield; see Scheme S1).

X-ray crystallography: Single crystals of the X-ray quality were grown from $CHCl_3$-Et_2O, from which a dark red-black, tablet-shaped one with dimensions of approximately 0.137 × 0.089 × 0.055 mm was selected and attached using Paratone-N oil to a fiberglass loop. The assembly was then mounted to the goniostat bathed in a cold N_2 stream. Intensity data were collected at 150K on a Bruker D8 Venture Mo-IS Photon-II diffractometer, λ=0.71073Å. Results of data collection and structure refinement are given in ESI.

Cell viability (MTT) assay: The protocol used for cell viability assay was adopted from our recent publication [23]. The keep experimental parameters are: (i) cells were first seeded at the density of 8×10^4 cells/mL in a 96-well plate each with a 100-µL cell suspension and then incubated for 24 hours at 37°C in 5% CO_2 atmosphere; (ii) the above cells were then treated with different amounts of [$(L_2Fe)_2(\mu\text{-}O)$] each dissolved in 100 µL of fresh medium, followed by incubation under the same conditions for 24 hours; (iii) 10 µL of MTT reagent was added to each well

containing the drug-treated cells and incubated for 2 hours at 37 °C, followed by addition of 100 μL of detergent to each well; and (iv) after the plate was kept in the dark for 2 hours at 37 °C, the absorbance was measured at 570 nm with a SpectraMax M4 microplate reader.

LIVE/DEAD cell viability assay: The LIVE/DEAD cell viability assay was performed using a LIVE/DEAD test kit (Molecular Probes). The experimental procedure was adopted from our recent publication. [23] Briefly, cells of A2780cis were cultured in RPMI medium for 24 hours at 37 °C and in 5% CO_2 atmosphere, followed by treating them with $[(L_2Fe)_2(\mu\text{-}O)]$ at the concentration of 1.0 μM and incubating the treated cells for 24 hours under the same conditions. After washing with 1X PBS and fresh RPMI each 2 times, a 5-μL solution of calcein AM in anhydrous DMSO (4 mM) and a 10-μL solution of ethidium homodimer-1 DMSO/water of 1:4 v/v (2 mM) were consecutively added to a 10-mL RPMI cell culture medium to prepare a LIVE/DEAD working solution. 2 mL of the above solution was carefully transferred to a Petri dish and incubated for 30 minutes at room temperature. Before the sample was examined under the fluorescence microscope, the medium was once again changed with the dye-free RPMI culture medium.

Cellular uptake of $[(L_2Fe)_2(\mu\text{-}O)]$: The protocol used for cellular uptake experiments was reported in one of our recent publications [23]. The main experimental steps include: (i) cells of A2780cis were seeded at the density of 4×10^5 cells/mL in a 6-well plate and incubated for 12 hours; (ii) the above cells were treated with two different concentrations of $[(L_2Fe)_2(\mu\text{-}O)]$, followed by incubation for 4 hours; (iii) cells were washed with 1X PBS 3 times, harvested and counted, followed by acid digestion with HNO_3 at room temperature overnight; and (iv) Fe contents were analyzed by AAS after the calcined iron oxides formed at 620 °C for 5 hours were dissolved in aqua regia and the solution volume was adjusted to the desired value.

Nuclear accumulation of [$(L_2Fe)_2(\mu$-O)]: The protocol used for nuclear accumulation experiments was adopted from the same recent publication [23]. The main experimental steps include: (i) cells of A2780cis were seeded at the density of 4×10^5 cells/mL in a 6-well plate and incubated for 12 hours; (ii) the above cells were treated with 8 μM of [$(L_2Fe)_2(\mu$-O)], followed by incubation for 4 hours; (iii) cells were washed with 1X PBS 3 times, harvested and counted, followed by centrifugation to dissociate the cell membrane; (iv) the isolated nuclei were digested with HNO_3 at room temperature overnight; and (iv) Fe contents were analyzed by AAS after the iron oxides formed at 620 °C for 5 hours were dissolved in aqua regia and the solution volume was adjusted to the desired value.

Mitochondrial accumulation of [$(L_2Fe)_2(\mu$-O)]: The protocol used for nuclear accumulation experiments was adopted from one of our recent publications [23]. The main experimental steps include: (i) cells of A2780cis were seeded at the density of 4×10^5 cells/mL in a 6-well plate and incubated for 24 hours; (ii) the above cells were treated with 8 μM of [$(L_2Fe)_2(\mu$-O)], followed by incubation for 4 hours; (iii) cells were washed with 1X PBS 3 times, harvested and counted, followed by isolation of mitochondria using the mitochondria isolation kit for mammalian cells (Thermo Scientific); (iv) the isolated mitochondria were digested with HNO_3 at room temperature overnight; and (iv) Fe contents were analyzed by AAS after the iron oxides formed at 620 °C for 5 hours were dissolved in aqua regia and the solution volume was adjusted to the desired value.

Determination of change in the mitochondrial membrane potential: The protocol used for nuclear accumulation experiments was adopted from the same publication [23]. The main experimental steps include: (i) cells of A2780cis were seeded at the density of 4×10^5 cells/mL in a 35-mm sterile glass bottom culture dish and incubated for 12 hours; (ii) the above cells were

treated with 8 μM of [$(L_2Fe)_2$(μ-O)] as the treatment group or $FeCl_3$ as the control group, followed by incubation for 24 hours; (iii) cells were washed with 1X PBS 3 times and incubated with a medium containing JC-1 dye (2 μM) for 20 minutes at 37 ^oC; and (iv) after the medium was replaced with 500 μL dye-free RPMI, the sample was examined under the fluorescence microscope.

Cell membrane permeabilization assay: The protocol used for cell membrane permeabilization assay was adopted from the same publication [23]. The main experimental steps include: (i) cells of A2780cis were seeded at the density of 2×10^4 cells/mL in a 35-mm sterile glass bottom culture dish and incubated for 12 hours; (ii) the above cells were treated with 8 μM of [$(L_2Fe)_2$(μ-O)] as the treatment group and or $FeCl_3$ as the control group, followed by incubation for 24 hours; (iii) cells were washed with 1X PBS 3 times and incubated with a medium containing PI dye (2 μM) for 20 minutes at 37 ^oC; and (iv) after the medium was replaced with 500 μL dye-free RPMI, the cells were examined under a fluorescence microscope.

Measurements of intracellular ROS: The protocol used for intracellular ROS measurements was adopted from the same recent publication [23]. The main experimental steps include: (i) cells of A2780cis were plated at the density of 2×10^4 cells/mL in a in black, clear-bottomed, 96-well plate and incubated for 12 hours; (ii) the above cells were treated with varying amounts of [$(L_2Fe)_2$(μ-O)], followed by the addition of 2′,7′-dichlorofluorescein diacetate (DCFH-DA) to the cell culture to reach the final concentration of 10 μM and incubated in dark for 30 minutes.; (iii) cells were washed with 1X PBS 2 times and resuspended in 100 μL of PBS; and (iv) the fluorescence intensity of solution was measured using a SpectraMax M4 microplate reader at the wavelength of 497/529 nm (Excitation/Emission).

Hemolysis assays: The hemolytic activity was carried out as reported previously.[29] Briefly, human blood cells (hRBCs) were treated with varying concentrations of [$(L_2Fe)_2(\mu\text{-}O)$], i.e., 2, 4, 8, 16, 32, 64 or 128 μM as the test group. Simultaneously, two other batches of hRBCs were treated with distilled water and Dulbecco's phosphate buffered saline (DPBS) as the positive and negative control group. Samples were incubated for 4 hours at 20 ºC and centrifugated for 5 minutes. Then, an aliquot of the supernatant 100 μL) from each sample was transferred to a 96-well plate, the absorbance at 577 nm of each sample was measured using a SpectraMax M4 microplate reader with the reference wavelength at 655 nm. The hemolysis ratio was obtained by the formula $(OD_{(test)} - OD_{(negative\ control)})/(OD_{(positive\ control)} - OD_{(negative\ control)}) \times 100\%$ to represent the degree of hemolysis.

Studies of Fe(II) release from [$(L_2Fe)_2(\mu\text{-}O)$]: The as-synthesized product of [$(L_2Fe)_2(\mu\text{-}O)$] (0.025 mM) dissolved in DMSO/ethanol was transferred to a UV-Vis cuvette. The reaction was then followed by UV-Vis spectroscopic measurements. In the absence of ascorbic acid, no change of spectroscopic features was detected, while an instantaneous change of spectroscopic features was recorded when ascorbic acid (0.025 mM) was added to the above mixture.

Statistical analysis: The statistical analysis was performed using GraphPad Prism (version 8.0). A two-tailed unpaired t-test was used to determine statistical significance of any two groups. After one-way ANOVA, the Holm-Sidak comparison test was carried out to calculate the statistical significance between groups. The results, expressed as mean ± standard error, were judged as statistically significant when P-value was less than 0.05.

3. Results and Discussion

The formation of **1** is a direct result of stereochemical hindrance of the ligand molecule, i.e., the methyl and Cl group on positions 2 and 8, respectively, prevents the formation of

tris(chlorquinaldolate)Fe(III) - our initial target molecule $Fe(L)_3$. Instead, the reaction between $Fe(NO_3)_3 \cdot 9H_2O$ with the ligand in the 1:3 ratio using K_2CO_3 as a base in wet ethanolic solution leads to the incorporation of a μ-O bridge into the product, forming a binuclear complex (**Scheme S1**). The elemental analysis (**Table S1**), UV-Vis (**Figure S1**), FT-IR (**Figure S2**) and single-crystal X-ray structure analysis showed that the isolated yellowish-brown crystalline product to be **1** with purity ≥97% on the basis of the Fe, C, H and N, HPLC (**Figure S3**) and ESI-HRMS (**Figure S4**) studies. **1** crystallizes in the triclinic space group $P\bar{1}$ with the asymmetric unit containing two similar Fe-L_2 moieties linked by a μ-O bridge, and the two moieties are not symmetry-related as all atoms are situated in general positions (**Table S2**). Nevertheless, both Fe(III) centers are each in a comparable distorted trigonal-bipyramidal coordination environment generated by two O- , two N- and the μ-O-donor atoms. Overall, the ionic character of each Fe(III) center is completely concealed in the deep pocket created by the lipophilic ligand molecules along with the μ-O bridge, making this binuclear Fe(III) complex reminiscent of the Fe(III)-transferrin complex (**Figure 1a** and **Figure 1b**). All bond lengths and bond angles in **1** were found to be normal (**Tables S3 - S6**).

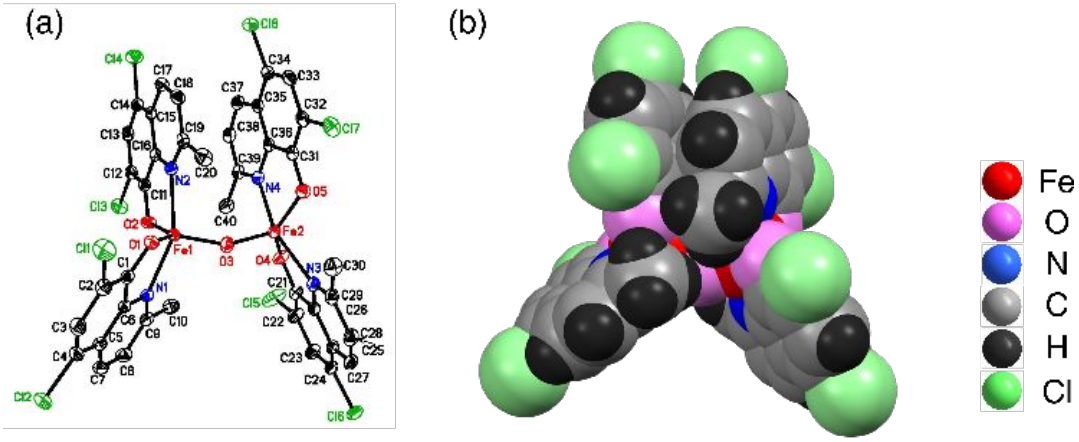

Figure 1. Molecular structure of **1** represented by (a) an ORTEP drawing (50% probability ellipsoids) and (b) a space-filling model.

The stability of **1** was tested in pure DMSO solution as well as in the cell culture medium containing DMSO (RPMI medium with 10% FBS and 1% antibiotics, pH-7.3, containing 1% DMSO) by means of time-dependent UV-Vis spectroscopic monitoring for a 24-hour and 72-hour incubation period, respectively, (see **Figures S5a – S5b**). These studies showed that no release of iron or ligand exchange occurred in either solution. Since the bidentate ligand L contains the O- and N-donor, chlorquinaldolate, as a hard-Lewis base, has higher affinity for Fe(III) over Fe(II). We investigated if Fe(II) could be released from **1** under the acidic and reductive conditions that are similar to the intracellular environment of bacteria. Both these aspects are the hallmark of transferrin-inspired Fe(III) delivery systems, i.e., the judicious selection of a hard-Lewis base as the ligand with high affinity for Fe(III) to prevent extracellular demetallation to unleash unwanted iron toxicity, while the soft-Lewis acid Fe(II) can be readily released from such ligand to harness intracellular iron toxicity. The results showed that when ascorbic acid was added to the solution of **1**, the release of Fe(II) was detected instantaneously by the appearance of the UV-Vis spectroscopic features of the pure ligand (see **Figure 2** and **Figure S6**).

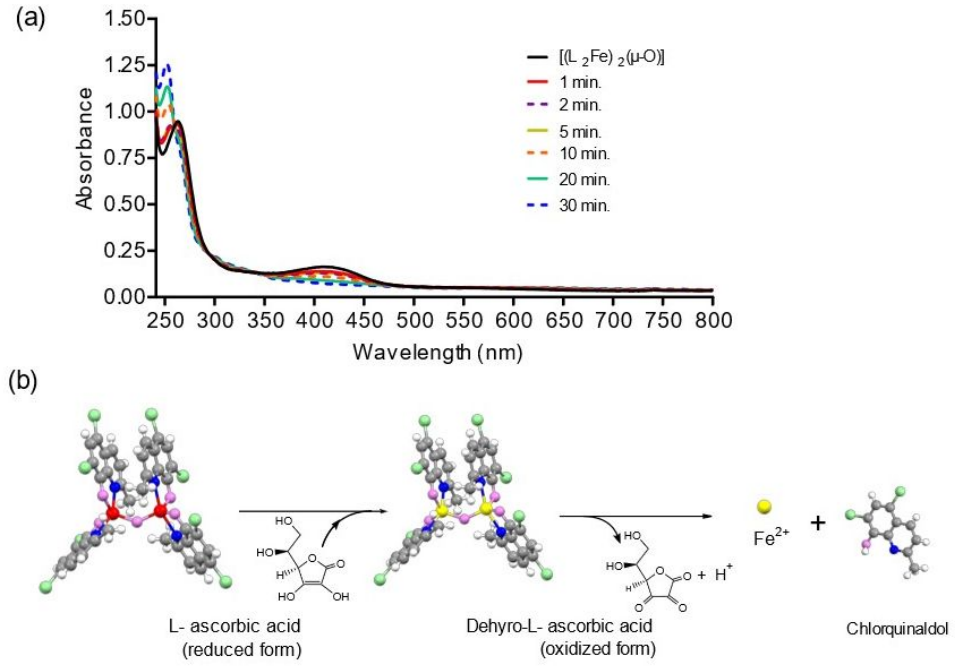

Figure 2. Results of Fe(II) release from **1** under the acidic and reductive conditions: (a) the spectroscopic evidence of Fe(II) release from **1** as detected by conversion of the UV-Vis spectra from **1** to chlorquinaldol, and (b) the schematic of Fe(II) release from **1** when ascorbic acid was used as a acidifying and reducing agent.

We then examined the *in vitro* anticancer activity of **1** against six different cancer cell lines using the MTT assay. The six cancer cell lines are: (1) A2780 (Pt-sensitive ovarian cancer cells), (2) A2780cis (Pt-resistant ovarian cancer cells), (3) SKOV-3 (ovarian cancer cells), (4) MDA-MB-231 (breast cancer cells), (5) MCF-7 (breast cancer cells), and (6) A549 (lung cancer cells). We measured the IC_{50} values against each of the above cancer lines by first treating the cells with **1** for 24 hours and then examined their viability. The results are summarized in **Figure 3a** with two representative killing curves, one against A2780 and another against A2780cis given in **Figure 3b**. Our results showed that in each of these six cancer cell lines, **1** exhibited a lower IC_{50} value than cisplatin. The *in vitro* efficacy ratio of IC_{50} for cisplatin *vs*. IC_{50} for **1**, a useful indicator of

cytotoxicity of **1** in comparison with that of cisplatin in cancer cells, ranges from 1.87 in A549 cells to 15.6 in A2780cis, signifying that **1** is a more potent anticancer agent than cisplatin against all these cancer cell lines. Furthermore, there are two different phenotypes of ovarian cancer cell lines, one is cisplatin-sensitive (i.e., A2780), and another is cisplatin-resistant (i.e., A2780cis) that have been commonly used to estimate the resistance factor (RF) in Pt-resistant cells for any given anticancer agent against such ovarian cancer cells using the IC_{50}(A2780cis)/IC_{50}(A2780) ratio as the indicator. Our results showed that **1** had an RF of 4.2, in sharp contrast to an RF of 13.8 for cisplatin, against these two cell lines, suggesting that **1** can overcome Pt resistance in ovarian cancer cells. It should be noted that RF of 4.2 for **1** is higher than RF of 1.5 for the ligand chlorquinaldol, suggesting a slight cross resistance in **1** - a metallodrug as compared with chlorquinaldol - a pure organic compound. The anticancer activity of **1** was further confirmed by a LIVE/DEAD cell assay. The A2780cis cells were first treated with **1** at the concentration of 1.0 μM for 24 hours, then stained with the assay stock containing a red fluorescent dye, ethidium homodimer (Erb) for dead cells and a green, fluorescent dye, calcein AM for live cells. Hence, the live cells would exhibit green fluorescence signals, and the dead cells would produce red fluorescence signals under the confocal fluorescence microscope. As shown in **Figure 3c**, our results of the LIVE/DEAD cell assay showed that the signal intensity of the red fluorescence was stronger than that of the green fluorescence, confirming the *in vitro* anticancer activity of **1**. In summary, **1** is not only more toxic than cisplatin to cancer cells, but also able to overcome Pt resistance in the phenotype of A2780cis cancer cells.

(a)

IC_{50} (μM)	A2780 Ovarian Cancer Sensitive to cisplatin	A2780cis Ovarian Cancer Resistant to cisplatin	SKOV-3 Ovarian Cancer	MDA-MB-231 Breast Cancer	MCF -7 Breast Cancer	A549 Lung Cancer	Resistance Factor $\frac{IC_{50}(A2780cis)}{IC_{50}(A2780)}$
Chlorquinaldol (L)	19.12 ± 1.52 μM	28.18 ± 1.34 μM	35.60 ± 1.75 μM	23.60 ± 0.75 μM	18.36 ± 1.24 μM	28.10 ± 1.57 μM	1.5
$[(L_2Fe)_2(\mu\text{-}O)]$;(**1**)	0.41 ± 0.05 μM	1.75 ± 0.15 μM	3.05 ± 0.20 μM	1.98 ± 0.23 μM	2.78 ± 1.51 μM	7.13 ± 1.23 μM	4.2
Cisplatin	1.98 ± 0.18 μM	27.33 ± 1.44 μM	33.93 ± 1.20 μM	24.64 ± 3.35 μM	21.37 ± 1.51 μM	13.38 ± 0.85 μM	13.8

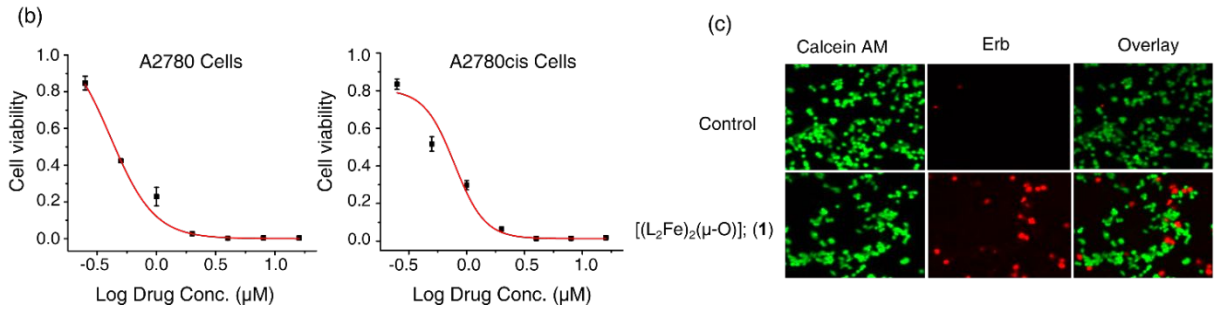

Figure 3. Results of *in vitro* anticancer activity studies on **1**: (a) IC_{50} values of ligand L, **1** and cisplatin against different cancer cell lines, (b) representative killing curves of **1** against two different phenotypes of ovarian cancer cell lines (i.e., A2780 *vs*. A2780cis), and (c) images of A2780cis cells treated with **1** and stained with Erb and calcein AM from the LIVE/DEAD assay kit.

To examine the cell membrane penetration of **1**, its cellular uptake was quantitatively measured by analyzing the intracellular Fe content of the cells treated with **1**. Specifically, the treatment group contained approximately one million A2780cis cells and were treated with **1** at two different concentrations, i.e., 8 μM and 16 μM. Similarly, the reference group contained the same number of cells and were treated with $FeCl_3$ at two corresponding molar concentrations as with **1**. After incubation for 4 hours, the cells were lysed, and the Fe contents were measured using atomic absorption spectrometry (AAS). As shown in **Figure 4a**, the cellular Fe content of the cells in that treatment group at the concentration of 8 μM was 1.5-fold higher (116.59 ± 13.89 nM/million cells) than that of the cells in the reference group (i.e., 76.14 ± 1.78 nM/million cells).

The difference of the intracellular Fe content became 2.5 times between the treatment group and reference group when a concentration of 16.0 μM of **1** or $FeCl_3$ was used, respectively, to treat the cells, i.e.,175.2 ± 5.19 nM/million cells in the treatment group *vs*. 77.6 ± 0.28 nM/million cells in the reference group. We also investigated whether **1** could penetrate the nucleus to cause oxidative damage to DNA, which can be even more detrimental to cancer cells. We treated A2780cis cells (4×10^5 cells/mL) with **1** at the concentration of 8 μM for 4 hours with the untreated cells as the control group. After the nuclei were isolated by centrifugation with 0.1% cell lysis buffer solution, we then analyzed the Fe contents by AAS. As shown in **Figure 4b**, the nuclei from the cells in the treatment group had a 4-fold increase of Fe content (i.e., 36.78 ± 2.65 nM/million cells) when compared with those from the cells in the control group (i.e., 8.36 ± 0.42 nM/million cells). The ability of **1** to overcome Pt resistance in A2780cis cells prompted us to investigate whether **1** could accumulate in mitochondria, which might provide insights into the remarkable *in vitro* anticancer activity of **1**. We again treated A2780cis cells (4×10^5 cells/mL) with **1** at the concentration of 8 μM with 4-hour incubation and used the untreated cells as the control group. We then isolated the mitochondria with an isolation kit (Cat no; 89878, Thermo Scientific™), the Fe contents in the isolated mitochondria were measured by AAS. As shown in **Figure 4c**, the mitochondrial uptake of **1** was more than 3 times higher in the treatment group (i.e., 86.87 ± 1.18 nM/million cells) than that in the control group (i.e., 28.01 ± 2.12 nM/million cells).

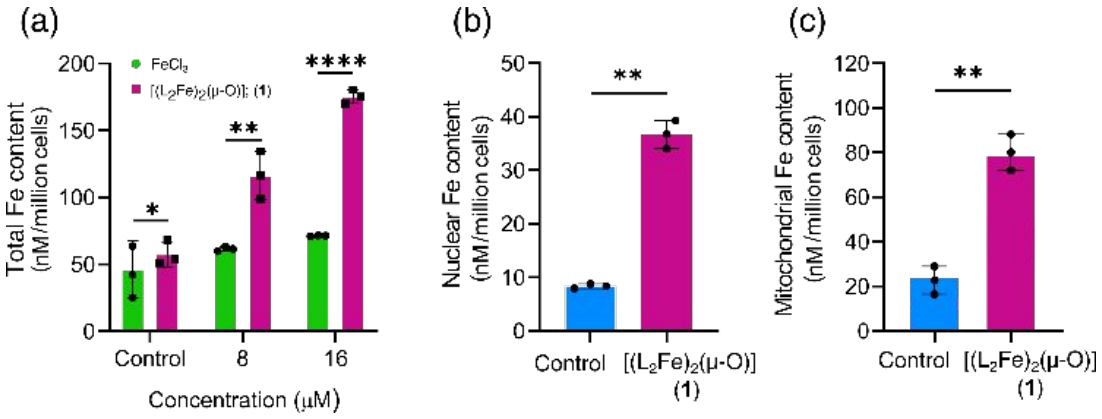

Figure 4. (a) The Fe contents in the cell lysates of the treatment group and reference group, (b) the nuclear Fe contents in the treatment group and the control group of A2780cis cells, and (c) the mitochondrial Fe contents in the treatment group and the control group of A2780cis cells (data presented as mean ± s.d, n =3 replicates; *p < 0.05, **p < 0.01, ***p < 0.001, ****p < 0.001 and ns = not significant).

The anticancer activity of **1** is most likely to stem from its ability to disrupt iron homeostasis in the intracellular free iron store. Such exogeneous iron in turn can trigger the Fenton reaction to produce ROS to cause damage to cellular proteins, DNA, and lipids, thus leading to cell death.[24] The Fenton reaction is a catalytic process where iron acting as a catalyst is not consumed but regenerated between steps 1 and 2. As a result, the net reaction is the splitting of hydrogen peroxide into two types of free radicals as shown in step 3. The standard reduction potential of Fe^{3+}/Fe^{2+} of 0.771 V makes iron the best catalyst for this process.

$$Fe^{2+} + H_2O_2 \rightarrow Fe^{3+} + HO\bullet + OH^- \quad [1]$$

$$Fe^{3+} + H_2O_2 \rightarrow Fe^{2+} + HOO\bullet + H^+ \quad [2]$$

$$2H_2O_2 \rightarrow HO\bullet + HOO\bullet + H_2O \quad [3]$$

We then conducted bioassays in A2780cis cells to measure the intracellular ROS generation triggered by **1** using the fluorescent probe 2,7-dichlorofluorescein diacetate (DCFH-DA). The

latter is a nonpolar cell permeable dye commonly employed to detect intracellular ROS generation. As shown in **Figure 5a**, the intracellular ROS generation in the A2780cis cells that were treated with **1** exhibited a dose-dependent escalation, strongly suggesting that the cell death in such cancer cells is primarily attributable to the ROS generation. We used thiourea (TU) - a well-known scavenger molecule of free radicals, to counter the effect of intracellular ROS generation.[25] The results showed that TU could protect the A2780 cells that were treated with **1** from the detrimental effect of ROS. Although the cell death was not entirely avoided using TU, this observation nevertheless showed that complete restoration of cell viability could not be achieved by scavenging intracellular ROS once they were generation (**Figure 5b**). On the other hand, 2,2´-bipyridine (bipy) is a chelating agent known to completely inhibit the Fenton catalytic activity by selectively chelating Fe(II) in the free iron store. We then used bipy to quench the intracellular ROS generation triggered by the Fe(II)-catalyzed Fenton reaction. The results demonstrated that bipy could completely protect A2780 cells treated with **1** from the deleterious effect of ROS and fully restore their viability (**Figure 5c**), suggesting that the Fenton catalytic reaction triggered by Fe(II) is responsible for the intracellular ROS production. We also examined the cell membrane integrity of A2780cis cells treated with **1** by measuring the change of membrane permeability using a propidium iodide (PI) staining uptake assay. We seeded the A2780cis cells at the density of 2×10^5 cells per well and treated the cells with **1** (1 μM) for 24 hours. After 100 μL of the medium containing PI dye at the final concentration of 2 μM was added to cells and incubated for 20 min at 37 ^{o}C, samples were immediately imaged using a confocal fluorescence microscope. The results showed that the uptake of PI dye in A2780cis cells that were treated with **1** was increased significantly as opposed to that in the untreated cells. Furthermore, cell membrane damage was also visible in the bright-field image of the cells in the treatment group when compared with those

in the control group, which indicates that the membrane-lytic activity of **1** is mostly likely a consequence of its ability to generate ROS (**Figure 5d**). The mitochondrial membrane potential of the A2780cis cells treated with **1** (2 μM) for 12 hours and stained with the cationic dye JC-1 was studied using confocal microscopy.[26] The treatment of A2780cis cells with **1** caused the reduction of mitochondrial membrane potential as revealed by the color change of the cells from red to green (see **Figure 5e**). Specifically, the ratio of red to green fluorescence intensity in the cells treated with $FeCl_3$ or in the untreated cells in the control group showed no statically significant change (**Figure 5f**). These results indicate that **1** can cause depolarization or/and disruption of the mitochondrial membrane function.

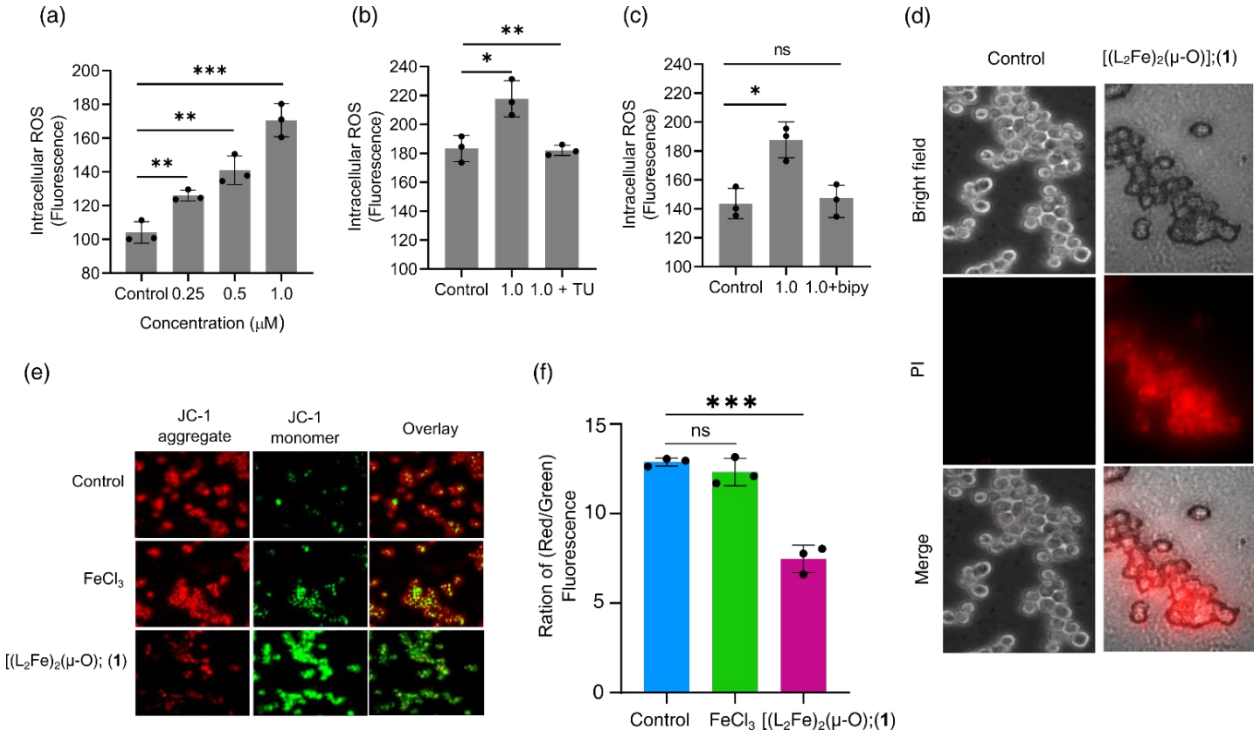

Figure 5. (a) Intracellular ROS generation in A2780cis cells treated with **1** of varying concentrations, (b) effect of scavenging free radicals by TU in A2780cis cells treated with **1**, (c)

effect of Fe(II) chelation by bipy in A2780cis cells treated with **1**, and (d) effect of **1** on the permeability of cell membrane in A2780cis cells treated with **1** at 1.0 μM in comparison with the untreated cells as the control; Differential interference contrasts microscopic (DIC) images from left to right: bright-field images, fluorescence images and merged images, (e) effect of **1** on mitochondrial membrane potential revealed by microscopic images of JC-1 fluorescent signals in the control group, the reference group with $FeCl_3$ and the treatment group (2.0 μM for both $FeCl_3$ and **1**), (f) the ratio of red to green fluorescence signal intensity in the control, reference and treatment group at the concentration of 2.0 μM for 12 hours (data presented mean ± s.d, n =3 replicates; *$p < 0.05$, **$p < 0.01$, ***$p < 0.001$ and ns = not significant).

Additionally, cytotoxicity of **1** in the wide concentration range of 2 μM to 128 μM was evaluated in human embryonic kidney cells (HEK 293) using the MTT assay. As shown in **Figure 6a**, cell viability of these noncancerous cells incubated with **1** for 24 hours was higher than 80% at the concentration of 128 μM, suggesting a relatively wide therapeutic window may exist in **1** for cancer treatment. These results suggest that noncancerous cells are more able than cancerous cells to counter the damaging effect of ROS. It is generally understood that non-enzymatic antioxidants such as glutathione, vitamin A, vitamin C, vitamin E, and antioxidant enzymes such as catalase, superoxide dismutase, and glutathione peroxidase work together in normal cells to maintain redox homeostasis.[27] On the other hand, malignant cells typically have increased ROS levels due to oncogenic activation, increased metabolic activity, and mitochondrial dysfunction.[28] As a result, increasing oxidative stress in malignant cells is more harmful to cancer cells since it can easily trigger apoptosis. Finally, we examined the hemolysis of **1** in human red blood cells (hRBCs) using the method we recently reported.[29] We observed that at the very high concentration of 128 μM, the hemolytic activity of **1** was negligible, i.e., <5% (**Figure 6b** and **Figure S7**). These preliminary results show that **1** might have a good safety profile for parenteral delivery as a systemic anticancer drug.

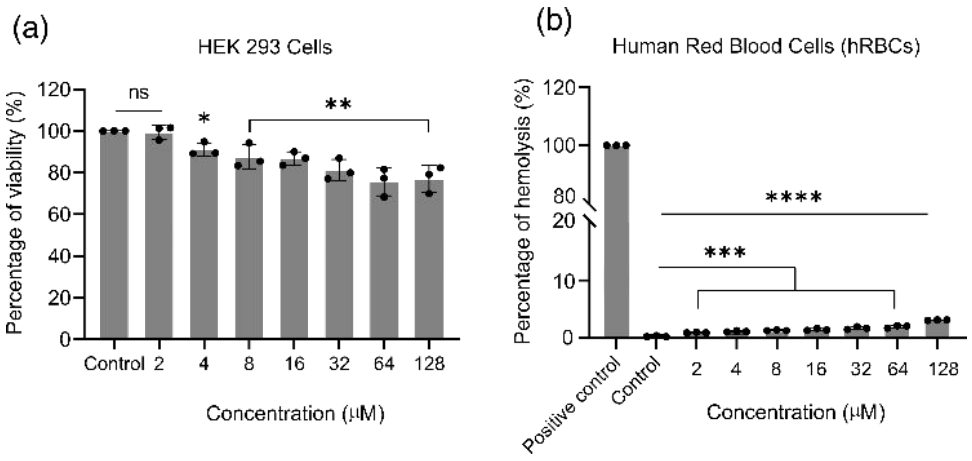

Figure 6. (a) Results of cell viability studies on **1** in human embryonic kidney cells (HEK 293) and (b) results of hemolytic studies in hRBCs (mean ± s.d, n = 3 replicates; *p < 0.05, **p < 0.01, ***p < 0.001. ***p < 0.001 and ns = not significant).

4. Conclusion

Our studies of **1** as an anticancer agent suggest that in order to successfully harness anticancer activity of iron, two major challenges need to be overcome. First, use of high lipophilic chelating agents that favor the formation of Fe(III) complexes over the Fe(II) counterparts is most critical to enhance the cell membrane penetration of the drug, while preventing any premature release of iron into the blood stream to cause cytotoxicity to normal tissues or/and hemolytic damage to red blood cells. Most of the existing Fe-based anticancer complexes reported in the literature thus far do not seem to meet this criterium. Second, complete intracellular release of iron from Fe(III) complexes would not only immediately trigger the Fenton reaction in the cancer cell, but also allow the exogenous iron to be promptly transported to the liver for processing, storage and secretion, thus avoiding any long-term cytotoxicity of iron. Some organometallic Fe-based anticancer compounds represented by ferrocenium analogues and Fe(II) Schiff-base complexes do

not possess the release mechanism imparted by the HSAB theory or other proper release mechanisms. In this regard, **1** appears to be an ideal candidate to fulfill both requirements, pointing to a new direction for the development of rationally designed Fe(III) complexes as anticancer agents. Currently, *in vivo* anticancer efficacy studies of **1** are under way in order to assess its translatability as a metallodrug for cancer therapy.

Funding Sources

Funding for the D8 Venture diffractometer was through NSF-MRI grant CHE-1625737.

Conflict of Interests

The authors declare no competing financial interest.

ACKNOWLEDGMENT

The authors would like to thank Dr. Mahinda Gangoda and Mrs. Wjdan Jogadi at the Department of Chemistry and Biochemistry, Kent State University for technical assistance.

References

[1] Pantopoulos, K.; Porwal, S. K.; Tartakoff, A.; Devireddy, L. Mechanisms of mammalian iron homeostasis. *Biochemistry* **2012**, *51* (29), 5705-5724.

[2] Kaplan, J. Mechanisms of cellular iron acquisition: another iron in the fire. *Cell* **2002**, *111* (5), 603-606.

[3] Dixon, S. J.; Stockwell, B. R. The role of iron and reactive oxygen species in cell death. *Nature chemical biology* **2014**, *10* (1), 9-17.

[4] Winterbourn, C. C. Toxicity of iron and hydrogen peroxide: the Fenton reaction. *Toxicology letters* **1995**, *82*, 969-974.

[5] Juan, C. A.; Pérez de la Lastra, J. M.; Plou, F. J.; Pérez-Lebeña, E. The chemistry of reactive oxygen species (ROS) revisited: outlining their role in biological macromolecules (DNA, lipids and proteins) and induced pathologies. *International Journal of Molecular Sciences* **2021**, *22* (9), 4642.

[6] Li, J.; Cao, F.; Yin, H.-l.; Huang, Z.-j.; Lin, Z.-t.; Mao, N.; Sun, B.; Wang, G. Ferroptosis: past, present and future. *Cell death & disease* **2020**, *11* (2), 88.

[7] Hentze, M. W.; Muckenthaler, M. U.; Andrews, N. C. Balancing acts: molecular control of mammalian iron metabolism. *cell* **2004**, *117* (3), 285-297.

[8] Ganz, T.; Nemeth, E. Regulation of iron acquisition and iron distribution in mammals. *Biochimica et Biophysica Acta (BBA)-Molecular Cell Research* **2006**, *1763* (7), 690-699.

[9] Pearson, R. Hard Acids Soft and Bases. *J. Am. Chem. Soc* **1963**, *85* (22), 3533-3539.

[10] Hancock, R. D.; Martell, A. E. Ligand design for selective complexation of metal ions in aqueous solution. *Chemical Reviews* **1989**, *89* (8), 1875-1914.

[11] Mackenzie, E. L.; Iwasaki, K.; Tsuji, Y. Intracellular iron transport and storage: from molecular mechanisms to health implications. *Antioxidants & redox signaling* **2008**, *10* (6), 997-1030.

[12] McKie, A. T.; Barrow, D.; Latunde-Dada, G. O.; Rolfs, A.; Sager, G.; Mudaly, E.; Mudaly, M.; Richardson, C.; Barlow, D.; Bomford, A. An iron-regulated ferric reductase associated with the absorption of dietary iron. *Science* **2001**, *291* (5509), 1755-1759.

[13] Steere, A. N.; Byrne, S. L.; Chasteen, N. D.; Mason, A. B. Kinetics of iron release from transferrin bound to the transferrin receptor at endosomal pH. *Biochimica et Biophysica Acta (BBA)-General Subjects* **2012**, *1820* (3), 326-333.

[14] Köpf-Maier, P.; Köpf, H.; Neuse, E. Ferricenium complexes: a new type of water-soluble antitumor agent. *Journal of cancer research and clinical oncology* **1984**, *108* (3), 336-340.

[15] Bouché, M.; Hognon, C.; Grandemange, S.; Monari, A.; Gros, P. C. Recent advances in iron-complexes as drug candidates for cancer therapy: reactivity, mechanism of action and metabolites. *Dalton Transactions* **2020**, *49* (33), 11451-11466.

[16] Wani, W. A.; Baig, U.; Shreaz, S.; Shiekh, R. A.; Iqbal, P. F.; Jameel, E.; Ahmad, A.; Mohd-Setapar, S. H.; Mushtaque, M.; Hun, L. T. Recent advances in iron complexes as potential anticancer agents. *New Journal of Chemistry* **2016**, *40* (2), 1063-1090.

[17] Jakupec, M. A.; Keppler, B. K. Gallium in cancer treatment. *Current Topics in Medicinal Chemistry* **2004**, *4* (15), 1575-1583.

[18] Timerbaev, A. R. Advances in developing tris (8-quinolinolato) gallium (III) as an anticancer drug: critical appraisal and prospects. *Metallomics* **2009**, *1* (3), 193-198.

[19] Chitambar, C. R. Gallium-containing anticancer compounds. *Future medicinal chemistry* **2012**, *4* (10), 1257-1272.

[20] Yang, T.; Zhang, Z.; Zhang, J.; Li, Y.; Li, W.; Liang, H.; Yang, F. Developing a gallium(III) agent based on the properties of the tumor microenvironment and lactoferrin: achieving two-agent co-delivery and multi-targeted combination therapy of cancer. *Journal of Medicinal Chemistry* **2023**, *66*, 793-803.

[21] Man, X.; Yang, T.; Li, W.; Li, S.; Xu, G.; Zhang, Z.; Liang, H.; Yang, F. Developing a gadolinium(III) compound based on apoferritin for targeted magnetic resonance imaging and dual-modal therapy of cancer. *Journal of Medicinal Chemistry* **2023**, *66*, 7268-7279.

[22] Qi, J.; Gou, Y.; Zhang, Y.; Yang, K.; Chen, S.; Liu, L.; Wu, X.; Wang, T.; Zhang, W.; Yang, F. Developing anticancer ferric prodrugs based on the N-donor residues of human serum albumin carrier IIA subdomain. *Journal of Medicinal Chemistry* **2016**, *59*, 7497-7511.

[23] Abeydeera, N.; Stilgenbauer, M.; Pant, B. D.; Mudarmah, K.; Dassanayake, T. M.; Zheng, Y.-R.; Huang, S. D. Lipophilic Fe (III)-Complex with Potent Broad-Spectrum Anticancer Activity and Ability to Overcome Pt Resistance in A2780cis Cancer Cells. *Molecules* **2023**, *28* (13), 4917.

[24] Held, P. An introduction to reactive oxygen species. *Tech Resources-App Guides* **2012**, *802*, 5-9.

[25] Al-Anbaky, Q.; Al-Karakooly, Z.; Kilaparty, S. P.; Agrawal, M.; Albkuri, Y. M.; RanguMagar, A. B.; Ghosh, A.; Ali, N. Cytotoxicity of manganese (III) complex in human breast adenocarcinoma cell line is mediated by the generation of reactive oxygen species followed by mitochondrial damage. *International journal of toxicology* **2016**, *35* (6), 672-682.

[26] Sun, R. C.; Board, P. G.; Blackburn, A. C. Targeting metabolism with arsenic trioxide and dichloroacetate in breast cancer cells. *Molecular cancer* **2011**, *10* (1), 1-15.

[27] Trachootham, D.; Lu, W.; Ogasawara, M. A.; Valle, N. R.-D.; Huang, P. Redox regulation of cell survival. *Antioxidants & redox signaling* **2008**, *10* (8), 1343-1374.

[28] Liou, G.-Y.; Storz, P. Reactive oxygen species in cancer. *Free radical research* **2010**, *44* (5), 479-496. Weinberg, F.; Hamanaka, R.; Wheaton, W. W.; Weinberg, S.; Joseph, J.; Lopez, M.;

Kalyanaraman, B.; Mutlu, G. M.; Budinger, G. S.; Chandel, N. S. Mitochondrial metabolism and ROS generation are essential for Kras-mediated tumorigenicity. *Proceedings of the National Academy of Sciences* **2010**, *107* (19), 8788-8793.

[29] Abeydeera, N.; Yu, B.; Pant, B. D.; Kim, M.-H.; Huang, S. D. Harnessing the toxicity of dysregulated iron uptake for killing Staphylococcus aureus: reality or mirage? *Biomaterials Science* **2022**, *10*, 474-484.